NASA/TM-2000-210304

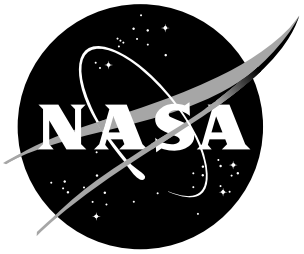

Mechanical Properties of LaRC™ SI Polymer for a Range of Molecular Weights

Karen S. Whitley, Thomas S. Gates, Jeffrey A. Hinkley, and Lee M. Nicholson
Langley Research Center, Hampton, Virginia

August 2000

The NASA STI Program Office ... in Profile

Since its founding, NASA has been dedicated to the advancement of aeronautics and space science. The NASA Scientific and Technical Information (STI) Program Office plays a key part in helping NASA maintain this important role.

The NASA STI Program Office is operated by Langley Research Center, the lead center for NASA's scientific and technical information. The NASA STI Program Office provides access to the NASA STI Database, the largest collection of aeronautical and space science STI in the world. The Program Office is also NASA's institutional mechanism for disseminating the results of its research and development activities. These results are published by NASA in the NASA STI Report Series, which includes the following report types:

- TECHNICAL PUBLICATION. Reports of completed research or a major significant phase of research that present the results of NASA programs and include extensive data or theoretical analysis. Includes compilations of significant scientific and technical data and information deemed to be of continuing reference value. NASA counterpart of peer-reviewed formal professional papers, but having less stringent limitations on manuscript length and extent of graphic presentations.

- TECHNICAL MEMORANDUM. Scientific and technical findings that are preliminary or of specialized interest, e.g., quick release reports, working papers, and bibliographies that contain minimal annotation. Does not contain extensive analysis.

- CONTRACTOR REPORT. Scientific and technical findings by NASA-sponsored contractors and grantees.

- CONFERENCE PUBLICATION. Collected papers from scientific and technical conferences, symposia, seminars, or other meetings sponsored or co-sponsored by NASA.

- SPECIAL PUBLICATION. Scientific, technical, or historical information from NASA programs, projects, and missions, often concerned with subjects having substantial public interest.

- TECHNICAL TRANSLATION. English-language translations of foreign scientific and technical material pertinent to NASA's mission.

Specialized services that complement the STI Program Office's diverse offerings include creating custom thesauri, building customized databases, organizing and publishing research results ... even providing videos.

For more information about the NASA STI Program Office, see the following:

- Access the NASA STI Program Home Page at ***http://www.sti.nasa.gov***

- E-mail your question via the Internet to help@sti.nasa.gov

- Fax your question to the NASA STI Help Desk at (301) 621-0134

- Phone the NASA STI Help Desk at (301) 621-0390

- Write to:
  NASA STI Help Desk
  NASA Center for AeroSpace Information
  7121 Standard Drive
  Hanover, MD 21076-1320

NASA/TM-2000-210304

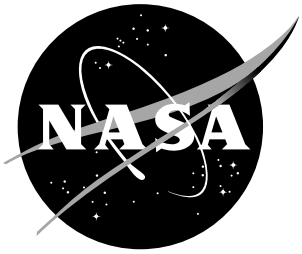

Mechanical Properties of LaRC™ SI Polymer for a Range of Molecular Weights

Karen S. Whitley, Thomas S. Gates, Jeffrey A. Hinkley, and Lee M. Nicholson
Langley Research Center, Hampton, Virginia

National Aeronautics and
Space Administration

Langley Research Center
Hampton, Virginia 23681-2199

August 2000

Available from:

NASA Center for AeroSpace Information (CASI)
7121 Standard Drive
Hanover, MD 21076-1320
(301) 621-0390

National Technical Information Service (NTIS)
5285 Port Royal Road
Springfield, VA 22161-2171
(703) 605-6000

Introduction:

When designing structural components based upon advanced polymeric materials, it would be desirable to understand how the intrinsic properties of a polymer (e.g. molecular weight, cross-link density, and free volume) affect mechanical performance at the macroscopic level. For optimum design of structural components using the polymer of interest, these intrinsic properties, which can be controlled during synthesis, would be selected prior to investing large amounts of resources in scale-up and fabrication. As shown in Noor, et al. [1] this approach could then be made part of a larger, multidisciplinary approach to design, which addresses the full breadth of length and time scales.

Unfortunately, current technology does not provide the polymer chemist or the component designer with the range of predictive methods that allow this judicious selection of these intrinsic properties. Recent advances in computer simulation methods (Abelson [2]) and the use of coarse structure-property relationships (Collantes, et al. [3]) show promise as methods that allow rapid determination of fundamental polymer properties based upon knowledge of the chemistry of the system. At the other end of the spectrum, analytical and numerical implementation of constitutive models such as in Schapery [4], Gates, et al. [5], and Jones [6] have proven successful in predicting thermal-mechanical performance based upon engineering level material property inputs. In between these types of modeling efforts exists a dearth of knowledge on how to use the intrinsic properties in a scheme that allows for the prediction of material static and time-dependent mechanical behavior.

One of the first steps in the construction of such models is the careful experimental correlation of thermal-mechanical behavior of a well-characterized polymer to known changes in intrinsic properties. Data from experiments provides insights into analysis model development as well as the basis for material properties required by the selected model. This data can also be cast into a form suitable for design guides and parametric studies.

Toward this end, the objective of this report is to detail and summarize the testing of an advanced polymer (LaRC^{TM}-SI). Elastic and inelastic tests were performed on this material over a range of temperatures below the glass transition with five known variations in molecular weight. Results from these tests will be presented along with descriptions of the material, experimental apparatus, and test methods.

Background:

Experiments on polymers such as atactic polystyrene as outlined by Nielsen [7] have shown that below the glass transition temperature (T_g), as the experimental regimen moves from elastic to viscoelastic to large strain and finally to fracture testing, the relative effect of molecular weight on mechanical properties increases. Support for this is given in recent room temperature experiments by Yost, et al. [8] on LaRC^{TM}-SI which have shown only a weak dependence of elastic properties (e.g. Young's modulus, shear modulus, Poisson's ratio) on molecular weight. Data from Matsuoka [9] showed that at or above the equilibrium state, the last two stages of stress relaxation are dependent upon molecular weight. Motivated by the desire to optimize the mechanical properties, Ward [10] studied the dependence of room temperature modulus, tensile strength and elongation on changes in molecular weight of a commercial thermoset resin. Results from this work indicated that strength and elongation were directly related to molecular weight. Nicholson, et al. [11] also showed the need for accurate analysis methods to predict the effects of molecular weight on properties such as fracture toughness.

Other studies by Matsuoka [9] noted that in the glassy state, the molecular weight affected the toughness and impact strength of the polymer where the impact strength increased with molecular weight. Similar results were also reported by Helminiak and Jones [12] on compact tension fracture tests for a family of thermosets and thermoplastics. Walsh and Termonia [13] studied the dependence of fracture toughness on molecular weight and test temperature for poly(methyl methacrylate) (PMMA). Only the intermediate molecular weights of PMMA exhibited fracture toughness decreasing with increasing test temperature. Failure studies on polystyrene Latex films by Sambasivam, et al. [14] also demonstrated that strength increased as the molecular weight increased. A study by Hallam, et al. [15] found that the molecular weight distribution affected the tensile strength of melt-spun and drawn linear polyethylene fibers. Polymer fibers of the same weight-average molecular weight ($\overline{M_w}$) showed that the distribution of molecular weights affected the fiber tenacity, with a low polydispersity increasing fiber tenacity.

Material Parameters and Test Specimens:

The material used in this study, LaRC™ SI (NASA Langley Research Center Soluble polyImide), was formulated with five different molecular weights. The polyimide was synthesized from 4,4'-oxydiphthalic anhydride (ODPA), 3,3',4,4'-biphenylcarboxylic dianhydride (BPDA) and 3,4'-oxydianiline (3,4'-ODA). Additional descriptions of this material can be found in Bryant [16]. The molecular weight variations, as demonstrated by Siochi, et al. [17], were designated by their percent offsets, one through five, and were purchased in the form of a powder where the variations in molecular weights were achieved through the use of percentage stoichiometric imbalances. The weight-average molecular weight ($\overline{M_w}$) and the number-average molecular weight ($\overline{M_n}$) corresponding to their percent offsets are given in table 1. The powder was dried under vacuum at 215°C for 48 hours to remove any residual solvents prior to molding into 152 x 152 mm neat resin plaques at 340°C for one hour under 3.1 MPa of pressure. The plaques were cut into specimens measuring approximately 150 x 17.5 x 5.8 mm to be used for static tensile tests.

Table 1. Molecular weight values per percent offset.

% offset	$\overline{M_w}$ (g/mol)	$\overline{M_n}$ (g/mol)
1	51070	11180
2	41100	13770
3	24290	10560
4	21180	10405
5	15880	8882

Test Conditions and Methods:

Monotonic Uniaxial Tensile Tests

Monotonic tensile tests were performed at six specific temperature intervals relative to the glass transition temperature (T_g) as shown in table 2. The goal of the tests was to

experimentally determine elastic properties, inelastic elongation behavior, and notched tensile strength as a function of molecular weight and test temperature. The T_g was determined prior to test for each molecular weight on the cured neat resin by using a Differential Scanning Calorimeter (DSC).

Table 2. Static Test Temperatures, °C

% Offset	T_g (°C)	Test Temperatures, °C				
		ΔT=15°C	ΔT=25°C	ΔT=45°C	ΔT=70°C	** ΔT=120°C
1	250	235	225	205	180	130
2	246	231	221	201	176	126
3	238	223	213	193	168	118
4	238	223	213	193	177*	126*
5	234	219	209	189	164	114

(ΔT = Tg - Test Temperature)

*The actual test temperatures deviated from ΔT.

** Corresponds to room temperature.

Uniaxial tensile tests were performed using a 22,200 N servo-hydraulic test system equipped with a heated test chamber. The specimens were enclosed in the chamber and mounted in mechanical wedge type grips. During the course of a test, temperature was monitored with several thermocouples placed near the specimen. The test temperature was stabilized first and then a tensile load was applied at a constant ramp rate of 22.2 N/sec. The tests were terminated when failure occurred or when the desired elongation was achieved.

As shown in figure 1, a high-temperature strain gage type, Measurements Group WK-00-250BG-350, was applied to each specimen in a direction transverse to the length prior to test. The specimen and gage were subsequently dried at 110°C for 120 hours and post-cured at 210°C for 2 hours. Specimens were then stored in a desiccator. Longitudinal strain was measured using a high temperature extensometer mounted along the edge of the specimen. Gage length of the extensometer was 25 mm and the signal was conditioned and collected using the test instrumentation. The output voltages from the strain gages were filtered and amplified by a strain gage conditioner before the conditioned output was collected by a digital data acquisition system.

Nominal engineering stress on the specimen was determined by dividing the load measured by the load cell by the average specimen cross-sectional area measured prior to the test. Each recorded measurement is an average of at least three replicates of a specimen with a given molecular weight offset at each test temperature.

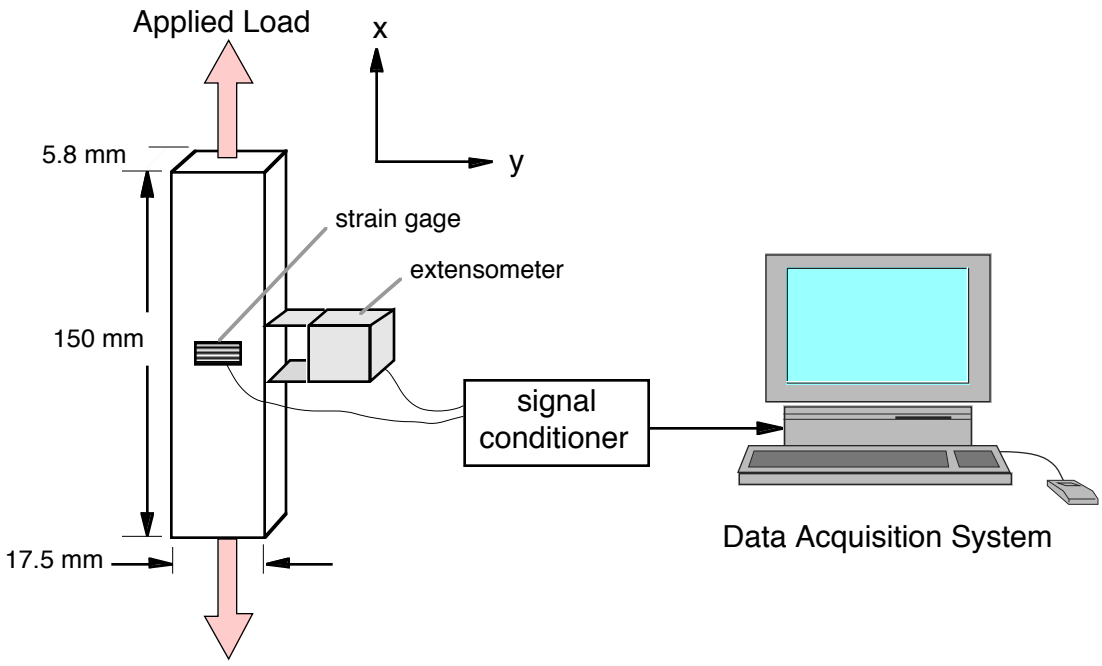

Figure 1: Schematic of the static test setup.

Notched Tensile Strength Test

For a given molecular weight, at least two tests at each temperature were conducted using a notched specimen geometry shown in figure 2. To facilitate a controlled failure, the notch was cut perpendicular to the specimen edge using a jeweler blade mounted on a handsaw. The notch was located on only one edge at 44 mm. from the bottom grip and extended approximately 2 mm. in from the free edge. Tensile strength was calculated by dividing the maximum load achieved during the tensile test by the nominal, unnotched specimen cross sectional area. Photomicrographs were taken of the notched surface after failure to determine the morphology of the failure surface. For each test condition and material offset, photomicrographs of the fractured surfaces were taken with an optical microscope at a magnification of 25X. Incident light was used for the photographs and no surface preparation was performed prior to examination.

Coefficient of Thermal Expansion

The coefficient of thermal expansion (CTE) for each specimen was measured with a laser dilatometer, [18]. Specimen geometry was rectangular and measured approximately 75 by 25 by 6 mm. Displacement was recorded at specific temperature intervals for a range of 21.1^{o}C to 143.3^{o}C. The CTE was calculated as the slope of the linear best fit to the data over the entire temperature range.

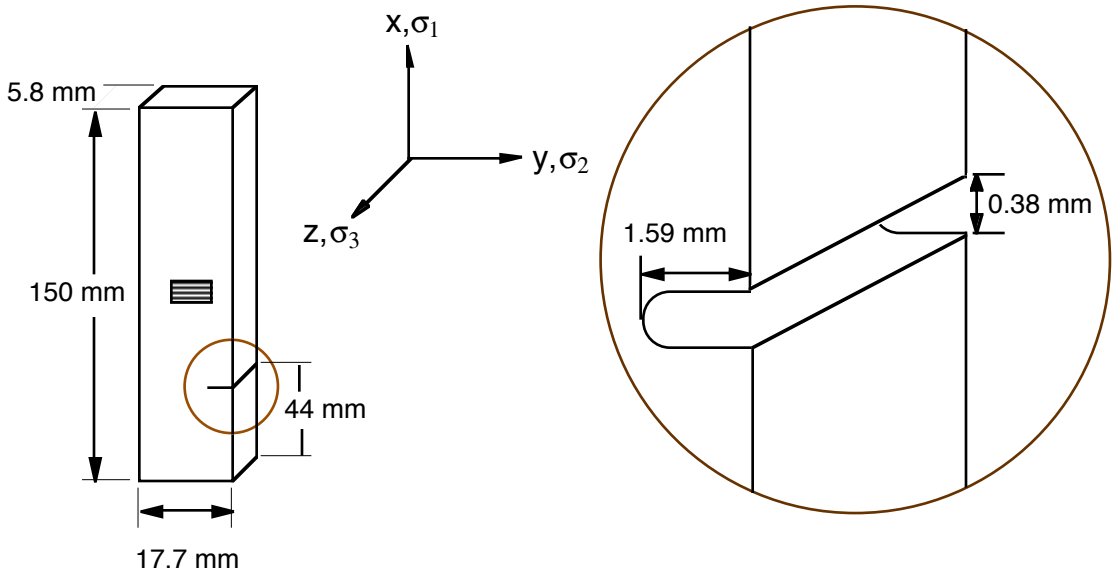

Figure 2. Notched specimen geometry.

Elastic Properties:

Young's Modulus (E) was calculated using equation (1) from the slope (least squares fit) of the linear portion of the longitudinal stress (σ_x) versus the longitudinal strain (ε_x) curve. Similarly, Poisson's Ratio, (ν) given by equation (2), was calculated as the slope of the transverse strain (ε_y) and the longitudinal strain in the same linear region. Shear modulus (G) given by equation (3), was calculated using the above values for E and ν. Subscripts in these equations refer to the specimen coordinate system (figure 1).

$$E = \frac{\sigma_x}{\varepsilon_x} \tag{1}$$

$$\nu = -\frac{\varepsilon_y}{\varepsilon_x} \tag{2}$$

$$G = \frac{E}{2(1+\nu)} \tag{3}$$

Inelastic Behavior:

For all static test specimens, the entire stress-strain data during loading was generated. In many cases, the notched specimens exceeded 2% strain to failure. For a given molecular weight, at least one unnotched specimen at each temperature was tested to high inelastic strain levels of at least 2% strain. The combined data sets from the notched and unnotched tests were used to characterize the inelastic behavior of the resin.

Yield Surface

As shown by Mendelson [19], the applied stress can be broken down into deviatoric and mean components. The deviatoric component is a function of the principal stresses which can be denoted as $(\sigma_1, \sigma_2, \sigma_3)$ where the subscripts refer to the principal directions of the material. Examining the invariants of the stress deviator tensor gives the classical J_2 invariant.

$$J_2 = \frac{1}{6}\left[(\sigma_1 - \sigma_2)^2 + (\sigma_2 - \sigma_3)^2 + (\sigma_3 - \sigma_1)^2\right] \qquad (4)$$

At the macroscopic level, it is assumed that the material is isotropic (Sternstein, [20] and [21]). This assumption is based on the fact that although there may be some low-level anisotropy at sub-molecular scales, this does not greatly influence macroscopic bulk properties at relatively low strains and at temperatures below the glass transition. Since it was assumed that the resin material was an isotropic material it behaved according to the Von-Mises yield condition (Mendelson [19]) such that in simple tension, we have

$$\sigma_o \equiv \textit{yield stress}$$

and that for yielding during tension loading in the 1 direction only, the principal stresses are now given by

$$\sigma_1 = \sigma_o, \quad \sigma_2 = 0, \quad \sigma_3 = 0 \qquad \text{(uniaxial)} \qquad (5)$$

such that the J_2 function is now given simply as

$$J_2 = \frac{1}{3}\sigma_o^2 \qquad (6)$$

Using these results, the equation (4) now can be written as:

$$\sigma_o^2 = \frac{1}{2}\left[(\sigma_1 - \sigma_2)^2 + (\sigma_2 - \sigma_3)^2 + (\sigma_3 - \sigma_1)^2\right] \qquad (7)$$

For biaxial loading, the out-of-plane stress vanishes such that

$$\sigma_1 \neq 0, \quad \sigma_2 \neq 0, \quad \sigma_3 = 0 \qquad \text{(biaxial)} \qquad (8)$$

and we now have the form:

$$\sigma_o^2 = \sigma_1^2 - \sigma_1\sigma_2 + \sigma_2^2 \qquad (9)$$

Plotting this equation in the (σ_1, σ_2) principal stress space gives the Von-Mises ellipse which describes the yield surface for any general case of in-plane loading. It is also assumed that the material is isotropic and homogeneous so that for yielding during tension loading in the 2 direction,

$$\sigma_1 = 0, \quad \sigma_2 = \sigma_o, \quad \sigma_3 = 0 \qquad (10)$$

and that for the pure shear case where

$$\sigma_1 = -\sigma_2 = k, \quad \sigma_3 = 0 \qquad \text{(shear)} \qquad (11)$$

we have

$$J_2 = \sigma_1^2 = k^2 \qquad (12)$$

Combining equation (6) and (12) gives

$$k^2 = \frac{1}{3}\sigma_o^2 \qquad (13)$$

$$k = \sigma_o / \sqrt{3} \tag{14}$$

This implies that the yield stress in pure shear is $(1/\sqrt{3})$ times the yield stress for uniaxial tension.

Stress-Strain Relations

In an isotropic material the total strain in the specimen can be decomposed into an elastic and a plastic incremental strain component.

$$d\varepsilon = d\varepsilon^e + d\varepsilon^p \tag{15}$$

where ε^e is the elastic strain and ε^p is the plastic strain. The elastic strain tensor can be written in terms of the elastic material properties

$$\begin{Bmatrix} \varepsilon_{11} \\ \varepsilon_{22} \\ \gamma_{12} \end{Bmatrix}^e = \begin{bmatrix} 1/E & -\nu/E & 0 \\ -\nu/E & 1/E & 0 \\ 0 & 0 & 1/G \end{bmatrix} \begin{Bmatrix} \sigma_{11} \\ \sigma_{22} \\ \sigma_{12} \end{Bmatrix} \tag{16}$$

where E, G, and ν are the elastic modulus, shear modulus, and Poisson's ratio, respectively. The subscripts refer to the material principal directions with the subscript 12 denoting in-plane shear.

For an isotropic, work hardening material such as LaRC™ SI, we assume that the plastic strain is a function of the applied stress so that

$$\varepsilon^p = \varepsilon - \varepsilon^e = f(\sigma, \beta) \tag{17}$$

where β represents material constants. At yield, the applied stress is equal to the yield stress so that using equation (9) gives,

$$f(\sigma) = \sigma_o = \sqrt{\sigma_1^2 - \sigma_1\sigma_2 + \sigma_2^2} \tag{18}$$

Experimental Characterization:

The elastic constants were found experimentally by using the measured total strain and equations (1), (2), and (3). The plastic strain was then determined using a power law expression. This power law has two empirical constants (A) and (n) such that

$$\varepsilon^p = A\sigma^n \tag{19}$$

For the uniaxial loading case, the total stress-strain relationship is now given as

$$\varepsilon_x = \frac{\sigma_x}{E} + A\sigma_x^n \tag{20}$$

Stress strain data from replicate tests were used to determine the average modulus (*E*). The plastic strain constants (A) and (n) were evaluated using a least squares fit of the stress-strain curves for each test temperature through equation (20). Having obtained values for (A) and (n) for each test temperature, the average exponent, n, was calculated for the entire data set. This value for n was then used to re-fit the stress-strain curves with equation (20) and

consequently a new constant (A) was found for each temperature. These computed values of (*A*) can be found in table 3.

Table 3: Values of inelastic constant (A) in $(Mpa)^{-n}$ computed with a fixed value of n = 2.75

	Test Temperatures					
% Offset	RT	ΔT = 120°C	ΔT = 70°C	ΔT = 45°C	ΔT = 25°C	ΔT = 15°C
1	2.47E-08	6.28E-08	7.47E-08	2.79E-07	7.14E-07	2.06E-06
2	3.15E-08	5.03E-08	7.85E-08	1.31E-07	3.86E-07	1.86E-06
3	2.91E-08	6.98E-08	5.72E-08	1.05E-07	3.32E-07	7.87E-07
4	1.52E-08	3.79E-08	2.93E-08	1.15E-07	2.58E-07	1.60E-06
5	1.70E-08	9.34E-08	3.78E-07	7.45E-07	1.10E-06	1.63E-06

Yield Criteria

For experimental stress-strain data that is not designated to be used in design of critical components, the choice of the material yield criterion is somewhat arbitrary and it may be chosen to illustrate an observed characteristic such as ductile-to-brittle transitions. Examination of the experimental stress-strain curves led to the establishment of the following yield criteria:

$$assume\ \ yield\ \ when\ \left(\varepsilon^{p}/\varepsilon^{e}\right) \geq 0.05 \qquad (21)$$

Therefore, the yield stress (σ_o) can be found by solving numerically for the applied stress such that

$$\sigma = \sigma_o\ \ when\ \left[\frac{A\sigma^{n}}{(\sigma/E)}\right] = 0.05 \qquad (22)$$

Using equation (18) and the values of (*A*) and (*E*), given in tables 3 and 5, respectively, the computed yield stress was found for each test condition and has been listed in table 4.

Table 4: Computed yield stress in MPa for each offset at each test condition.

	Test Temperatures					
% Offset	RT	ΔT = 120°C	ΔT = 70°C	ΔT = 45°C	ΔT = 25°C	ΔT = 15°C
1	36.34	25.48	24.50	11.48	7.32	4.45
2	31.02	28.79	22.76	17.87	10.03	4.64
3	32.77	22.59	27.86	19.92	10.90	6.85
4	47.44	32.09	27.50	18.85	12.39	4.96
5	44.92	18.69	8.91	6.55	5.33	4.69

Experimental Results, Inelastic Behavior:

Inelastic material constants

The values for the inelastic constant (A) in table 3 are plotted as a function of molecular weight and temperature in figure 3, which presents (A) on a logarithmic scale as function of molecular weight. The value for (A) is fairly constant for molecular weights above 25,000 (g/mol) with a distinct shift occurring below the 25,000 (g/mol) range.

Using the same data set but setting (A) as a function of test temperature, figure 4 shows that with the exception of the 5% offset material, the data combines into a well-grouped set that increases significantly above the 175^{o}C temperature range.

Yield stress

The calculated yield stress from equation (18) can also be represented as a function of molecular weight or test temperature. Figure 5, which shows yield stress as a function of molecular weight, indicates that yield stress for a constant temperature varies very little above the 25,000 (g/mol) weight level. Below molecular weights of 25,000 (g/mol), the yield stress shifts dramatically for all test temperatures. Figure 6 is used to plot this same data set now with yield stress as a function of test temperature. With the exception of the 5% offset material, the data follows a similar trend in that above the 175^{o}C temperature range the yield stress decreases sharply with an increase in test temperature.

Yield surface

A Von-Mises type yield surface (Mendelson [19]) was calculated using equation (9) for each molecular weight and at each test temperature. These surfaces, plotted in the principal stress space and given in figures 7-11, illustrate the predicted change in yield surface for any general case of in-plane, tension loading. For most of the molecular weights, the yield surface evolves in a uniform manner as temperature increases. However, the 1% and 5% molecular weight offset materials show some non-uniformity of evolution of the yield surface with temperature. This non-uniformity is most severe for the 5% molecular weight offset material. For equivalent temperatures, there are also some differences in the yield surface due to changes in molecular weight. Figure 12 illustrates these differences by comparing the yield surfaces for the 1% and 2% molecular weight offset materials for 3 different test temperatures.

Notched Tensile Strength

Figure 13 provides the design plot for NTS. In this plot, the lines of constant ΔT and constant molecular weight (percent offset) are provided to give the reader a complete picture of the range of tensile strengths available. This plot can be used to predict the notched tensile strength for a range of molecular weight offsets over a range of temperatures from room temperature up to 15°C below the Tg. For example, if a parallel line was drawn halfway between the temperature lines of ΔT= 120°C and ΔT= 70°C, one would predict that the notched tensile strength of the 3.5% molecular weight offset material to be about 30 Mpa at ΔT=95°C.

Ductile and Brittle Behavior

The measured notched tensile strength (NTS) and the calculated yield stress data can be combined in a way (figure 14) that indicates the propensity of the material to fail in a ductile or a brittle manner. Figure 14 presents data (tables 4 and 9) for each offset condition with different test temperatures. For equally scaled axes, the 45^o line on this plot shows the demarcation between the two failure modes. For conditions above the 45^o line, the material will tend to yield first and fail in a ductile manner. For data below the 45^o line, the material tends to fail at the notch in a brittle manner. Figure 14 indicates that the 1%, 2%, and 3% molecular weight offset materials all fail in a ductile manner at all test temperatures while the 4% and 5 % offset materials tend to fail in a more brittle manner. Some of the data for the 4% and 5% offset materials lie on the 45^o line, which indicates that the failure mode is not strongly ductile or brittle.

Experimental Results, Uniaxial Tension:

The experimental results will be presented for the measured uniaxial tension behavior. All results have been examined by comparing the property of interest to variations in test temperature and molecular weight offset. To place equal emphasis on the results, the temperature is referenced to the difference between glass transition and test temperature.

$$\Delta T = T_g - T_{test}$$

Elastic Properties

Young's modulus (E) versus temperature is given in figure 15. As expected, the modulus decreases as temperature was increased. The rate of change of E with temperature is fairly uniform up to the range of (ΔT=25°C). The transition to the highest temperature (ΔT=15°C) was associated with a sharp decrease in modulus.

The dependence of E on molecular weight offset is given in figure 16 for all temperatures. A slight dependence on offset is evident at all temperatures with E increasing as offset increases. Table 5 provides the values of E for each temperature and offset.

Table 5: Values of E (GPa) for each offset at each ΔT.

	Test Temperatures					
% Offset	RT*	ΔT=120°C	ΔT=70°C	ΔT=45°C	ΔT=25°C	ΔT=15°C
1	3.764	2.755	2.480	2.502	2.150	1.777
2	3.893	2.778	2.685	2.457	2.293	1.830
3	3.828	3.060	2.587	2.535	2.303	2.191
4	3.836	3.049	2.837	2.550	2.369	1.898
5	3.773	3.188	2.878	2.501	2.434	2.056

*RT = Room Temperature

The dependence of shear modulus (G) on temperature is given in figure 17. In accord with Young's modulus, G decreases in a uniform manner as the temperature is raised until the range

between (ΔT=25º) and (ΔT=15ºC) is reached. The variations of G with molecular weight offset, figure 18, are also similar to the results for E given in figure 16. Shear modulus increases as offset increases for all temperatures. Table 6 provides the values of G for each temperature and offset.

Table 6: Values of G (GPa) for each offset at each ΔT.

	Test Temperatures					
% Offset	RT*	ΔT=120°C	ΔT=70°C	ΔT=45°C	ΔT=25°C	ΔT=15°C
1	1.359	0.990	0.898	0.904	0.793	0.654
2	1.367	1.005	0.958	0.891	0.833	0.678
3	1.367	1.084	0.956	0.920	0.841	0.789
4	1.356	1.093	1.036	0.906	0.836	0.694
5	1.367	1.139	1.032	0.924	0.884	0.761

*RT = Room Temperature

The coefficient of thermal expansion (CTE) as a function of percent offset is shown in figure 19 and is presented in table 7. CTE shows no variation with percent offset.

Table 7: Coefficient of thermal expansion

% Offset	Avg. CTE με/°C	Stdev. CTE
1	21.385	0.319
2	22.112	0.427
3	21.381	0.142
4	21.678	0.591
5	21.637	0.731

The values for Poisson's ratio are given in table 8.

Table 8. Poisson's Ratio

Temperature	1% Offset	2% Offset	3% Offset	4% Offset	5% Offset
RT	0.385±0.018	0.422±0.025	0.402±0.026	0.414±0.023	0.363±0.045
ΔT=120°C	0.389±0.007	0.386±0.005	0.399±0.014	0.397±0.013	0.390±0.034
ΔT=70°C	0.379±0.020	0.393±0.008	0.358±0.017	0.390±0.028	0.389±0.045
ΔT=45°C	0.386±0.036	0.379±0.010	0.368±0.014	0.444±0.126	0.356±0.026
ΔT=25°C	0.356±0.006	0.376±0.011	0.367±0.009	0.435±0.045	0.380±0.036
ΔT=15°C	0.358±0.018	0.350±0.011	0.382±0.023	0.390±0.103	0.342±0.056

Strength

Notched tensile strength (NTS) versus temperature and molecular weight offset are shown in figures 20 and 21, respectively. The data are also tabulated in table 9. Figure 20 illustrates a

strong dependence of NTS on temperature. In general, NTS decreases as temperature increases. Over the range from room temperature to $\Delta T=120^{o}C$ the 1% and 2% materials show a much lower rate of change in NTS compared to the 3%, 4%, and 5% materials. However, at the range from $\Delta T=70^{o}C$ to $\Delta T=15^{o}C$ the converse is true with the 3%, 4%, and 5% materials showing a lower dependency of NTS on temperature than the 1% and 2% materials.

Table 9: Notched tensile strength (MPa) for each offset at each ΔT

	Test Temperatures					
% Offset	RT*	ΔT=120°C	ΔT=70°C	ΔT=45°C	ΔT=25°C	ΔT=15°C
1	63.85	63.53	49.64	39.56	30.03	22.93
2	69.86	64.46	53.36	41.43	32.45	24.63
3	66.70	50.22	34.43	29.65	21.39	29.59
4	47.54	27.98	10.81	9.61	13.85	7.54
5	33.50	12.42	6.83	4.62	4.76	2.98

*RT = Room Temperature

The variation in NTS with respect to offset, as shown in figure 21, indicate an insignificant change in NTS due to an increase in offset from the 1% to 2% materials for all temperatures. Increasing the percent offset beyond 2% gives rise to large changes in NTS with a net change of over 60% occurring for the $\Delta T=120^{o}C$ case. All cases show a decrease in NTS as the percent offset is increased beyond 2%.

Additional evidence of the effects of temperature and percent offset is obtained by examination of the material failure surface. The photomicrographs of the notched surfaces after failure at different temperatures are provided in figure 22 for all materials. A failure surface was classified as ductile if the photomicrograph showed evidence of material elongation and smooth, glassy looking surfaces. A failure surface was classified as brittle if the photomicrograph showed evidence of sharp edges and multiple crack sites. Regarding the changes in NTS with temperature, the first and second row of photographs in figure 22 for the 1% and 2% materials, respectively, document the changes from a brittle failure mode to a ductile failure mode as the temperature is raised from room temperature to $\Delta T=120^{o}C$. For the 3% and 4% molecular weight offset materials, the third and fourth row respectively, show a change from brittle to ductile failure as the temperature reaches the two highest test values ($\Delta T=25^{o}C$, $15^{o}C$). The 5% material, the fifth row of photographs, shows an initial transition to ductile failure as temperature increases from $\Delta T=120^{o}C$ to $45^{o}C$ and another transition as the temperature increases from $\Delta T=25^{o}C$ to $15^{o}C$.

Examination of the photomicrographs of the failure surface as a function of percent offset reveals features that correlate with the results given in figure 21. At room temperature, the photographs in the first column of figure 22 show a gradual change from brittle to ductile failure as the percent offset is increased. By contrast, at the elevated temperatures, ($\Delta T=120$, 70, 45, 25, $15^{o}C$) a sharp change from ductile to brittle failure is observed as the offset is increased beyond 2%.

Inelastic Behavior

Inelastic stress-strain curves for the unnotched specimens are shown in figures 23-27 for all test conditions. In some cases two replicates for each test were performed, thus the curve shown is representative of two data sets. In several cases the total strain achieved during elongation exceeded the range of the measurement transducer. Therefore, in order to compare the effects of temperature and molecular weight on inelastic behavior, curves were evaluated and fitted with equation (1) up to a strain level of 1% or failure, whichever occurred first.

In general, all molecular weight offsets showed increases in material nonlinearity as temperature increased. This fact, coupled with decreases in elastic modulus as temperature increases, produced distinct families of stress-strain curves. Characterization of these curves using equation (19) provided the material coefficients given in table 3.

The degree of nonlinearity was affected by the molecular weight with the tendency for nonlinearity increasing as the percent offset decreased. Figures 28 and 29 illustrate this behavior by presenting the stress-strain curves for each offset at room temperature and at $\Delta T=15^{o}C$ respectively. For both cases the 1% offset material gave the highest level of material nonlinearity.

Conclusions:

Elastic and inelastic tests were performed on an advanced polymer (LaRC^{TM}-SI) over a range of temperatures below the glass transition with five known variations in molecular weight. Young's modulus and shear modulus decreased as the test temperature increased. Young's modulus and shear modulus increased only slightly as the molecular weight offset increased. However, the notched tensile strength (NTS) is a strong function of both temperature and molecular weight. NTS decreased as the test temperature increased, and NTS decreased as the percent offset increased beyond 2%. Yield stress is a strong function of temperature for the 3%, 4%, and 5% molecular weight offset materials. The material nonlinearity increased as test temperature increased. For most of the molecular weights, the yield surface evolved in a uniform manner as temperature increased. However, the 1% and 5% molecular weight offset materials showed some non-uniformity of evolution of the yield surface with temperature. There were also some differences in the yield surface due to changes in molecular weight as illustrated in figure 12. The data presented in figure 14 suggests that the 1%, 2%, and 3% molecular weight offset materials all fail in a ductile manner. The observed microstructure also helped to characterize the brittle to ductile transition as a function of molecular weight.

Acknowledgements:

The authors would like to acknowledge the expert technical assistant of Mr. C. E. Townsley, and the gel permeation chromatography performed by Dr. E. J. Siochi.

References:

[1] Noor, A. K., Spearing, S. M., Adams, W. W., and Venneri, S. L., "Frontiers of the Material World," in *Aerospace America*, vol. 36, pp. 24-31, 1998.

[2] Abelson, P. H., "Nanophase Chemistry," *Science*, Vol. 271, pp. 11, 1996.

[3] Collantes, E., Gahimer, T., Welsh, W. J., and Grayson, M., "Evaluation of Computational Chemistry Approaches for Predicting the Properties of Polyimides," *Computational and Theoretical Polymer Science*, Vol. 6, pp. 29-40, 1996.

[4] Schapery, R. A., "Inelastic Behavior of Composite Materials," *ASME Winter Annual Meeting*, *AMD-13*, C. T. Herakovich, Ed. Houston: ASME, pp. 122-150, 1975.

[5] Gates, T. S., Chen, J. L., and Sun, C. T., "Micromechanical Characterization of Nonlinear Behavior of Advanced Polymer Matrix Composites," *Composite Materials: Testing and Design (Twelfth Volume), ASTM STP 1274*, R. B. Deo and C. R. Saff, Eds.: American Society for Testing and Materials, pp. 295-319, 1996.

[6] Jones, R. M., *Mechanics of Composite Materials*. Washington, D.C.: Scripta Book Company, 1975.

[7] Nielsen, L. E., *Mechanical Properties of Polymers and Composites*, Vol. 1. New York: Marcel Dekker, 1974.

[8] Yost, W. T., Cantrell, J., H., Gates, T. S., and Whitley, K. S., "Effects of Molecular Weight on Mechanical Properties of the Polyimide, LaRC-SI," presented at Review of Progress in Quantitative NDE, San Diego, 1997.

[9] Matsuoka, S., *Relaxation Phenomena in Polymers*. Munich: Hanser, 1992.

[10] Ward, B. C., "Effects of molecular weight and cure cycle on the properties of compression molded Celazole PBI resin.," presented at Advanced Materials Technology '87, Thirty-second International SAMPE Symposium, Anaheim, CA, 1987.

[11] Nicholson, L. M., Whitley, K. S., Gates, T. S., Hinkley, J. A., "How Molecular Structures Affects Mechanical Properties of an Advanced Polymer," presented at 44th International SAMPE Symposium and Exhibition, Long Beach, CA, 1999.

[12] Helminiak, T. E. and Jones, W. B., "Influence of molecular weight on fracture behavior of polyphenylquinoxaline thermosets.," *Adhesive chemistry: Developments and trends*. New York: Plenum Press, pp. 525-532, 1984.

[13] Walsh, D. J. and Termonia, Y., "Mechanical Properties of Low Molecular Weight Polymers as a Function of Temperature," *Polymer Communications*, Vol. 29, pp. 90-92, April 1988.

[14] Sambasivam, M., Klein, A., and Sperling, L. H., "Molecular-Basis of Fracture in Polystyrene Films – Role of Molecular Weight," *Journal of Applied Polymer Science*, Vol. 58, No. 2, pp. 357-366, 1995.

[15] Hallam, M. A., Cansfield, D. L. M., Ward, I. M., and Pollard, G., "A study of the effect of molecular weight on the tensile strength of ultra-high modulus polyethylenes.," *Journal of Materials Science*, Vol. 21, pp. 4199-4200, 1986.

[16] Bryant, R. G., "LaRC-SI: a soluble aromatic polyimide," *High Performance Polymers*, Vol. 8, pp. 607-615, 1996.

[17] Siochi, E., J., Young, P. R., and Bryant, R. G., "Effect of Molecular Weight on the Properties of a Soluble Polyimide," presented at 40th International Society of Advanced Materials and Process Engineering Symposium, 1995.

[18] Tompkins, D. E.,Bowles D. E., Kennedy, W. R., "A Laser-Interferometric Dilatometer for Thermal-Expansion Measurements of Composites," *Experimental Mechanics*, Vol. 26, March 1986.

[19] Mendelson, A., *Plasticity: Theory and Application*. Malabar, Florida: Robert E. Krieger Publishing Company, 1968.

[20] Sternstein, S. S., Ongchin, L., and Silverman, A., *Applied Polymer Symposia*, Vol. 7, pp. 175, 1968.

[21] Sternstein, S. S. and Myers, F. A., *Journal of Macromolecular Science*, Vol. 8, pp. 539, 1973.

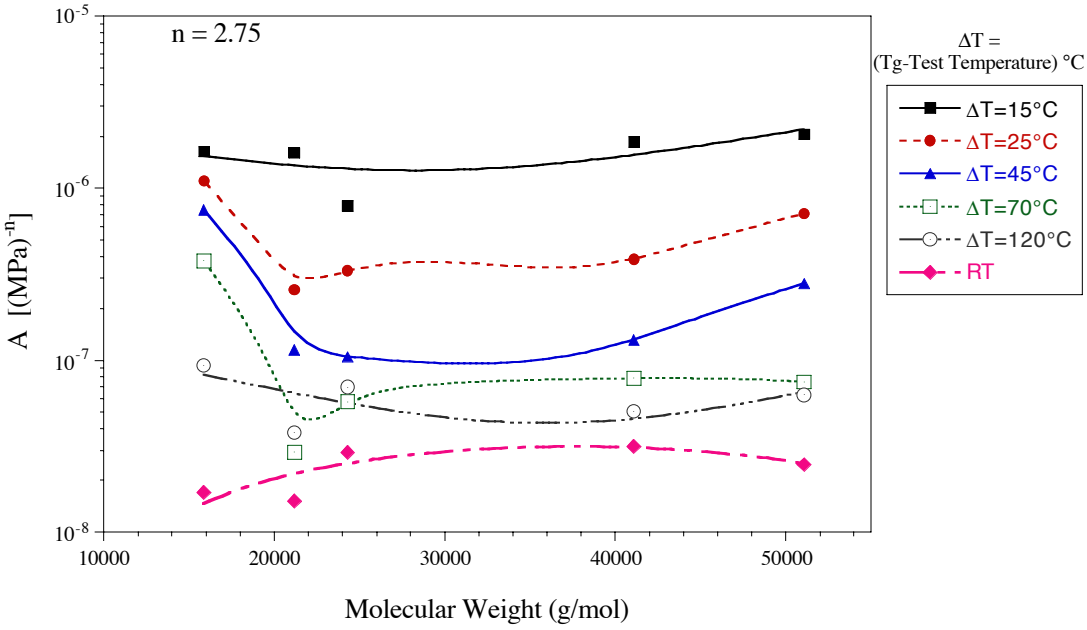

Figure 3: Inelastic constant (A) $[(MPa)^{-n}]$ as a function of molecular weight. (calculated with a constant n = 2.75)

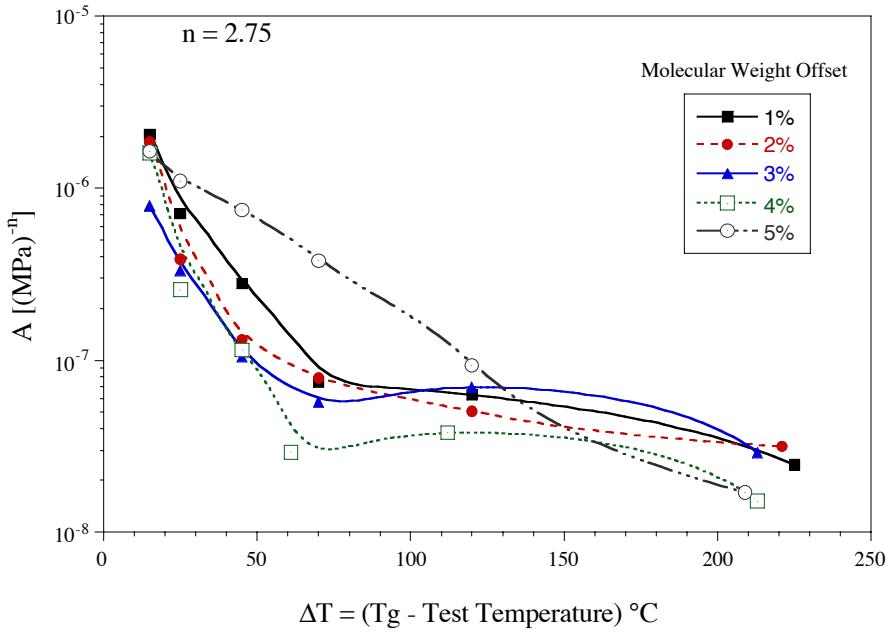

Figure 4: Inelastic constant (A) $[(MPa)^{-n}]$ as a function of temperature. (calculated with a constant n = 2.75)

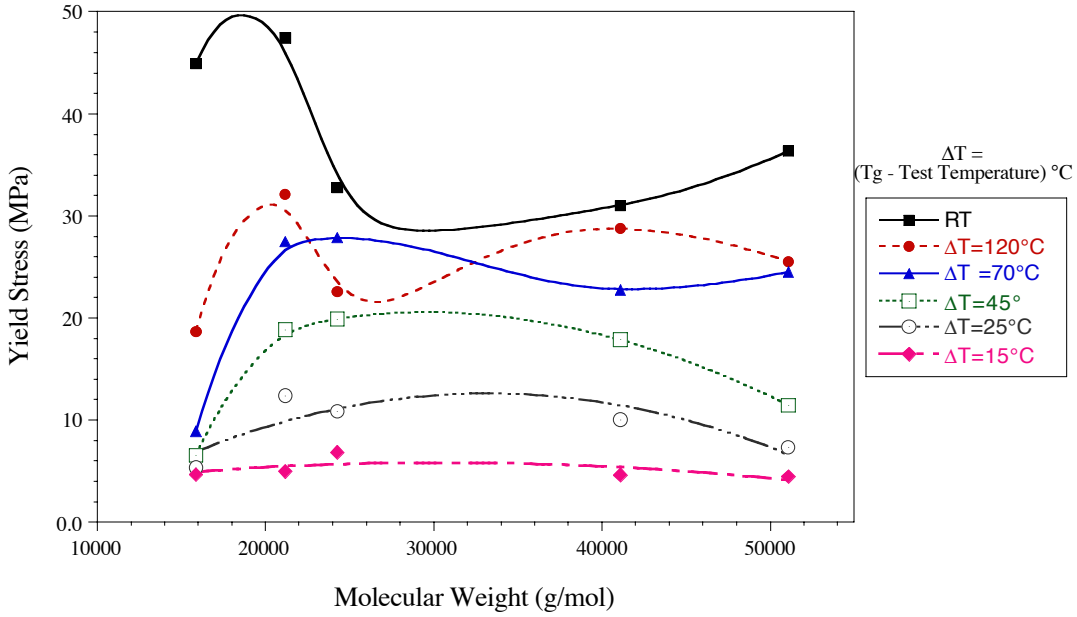

Figure 5: Yield Stress, σ_o (MPa), as a function of molecular weight.

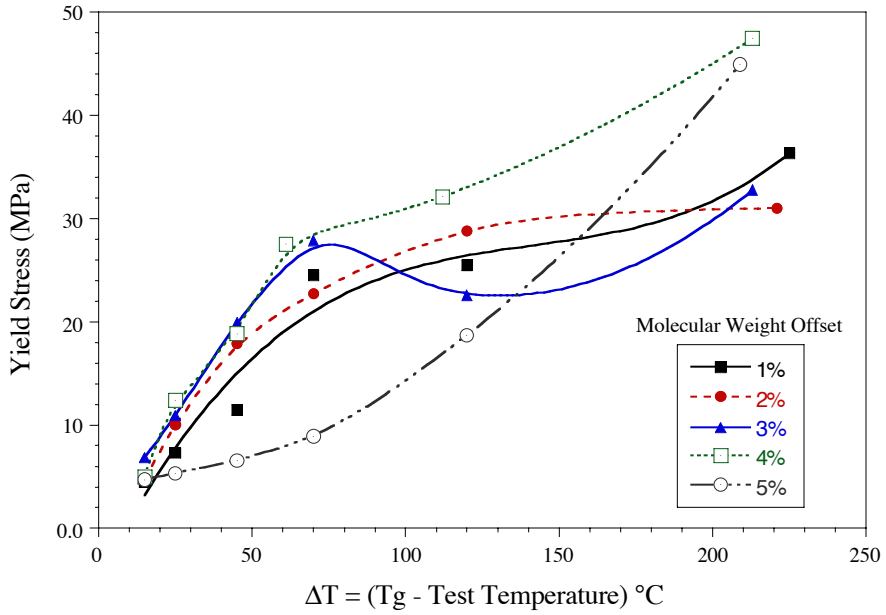

Figure 6: Yield Stress, σ_o (MPa), as a function of temperature.

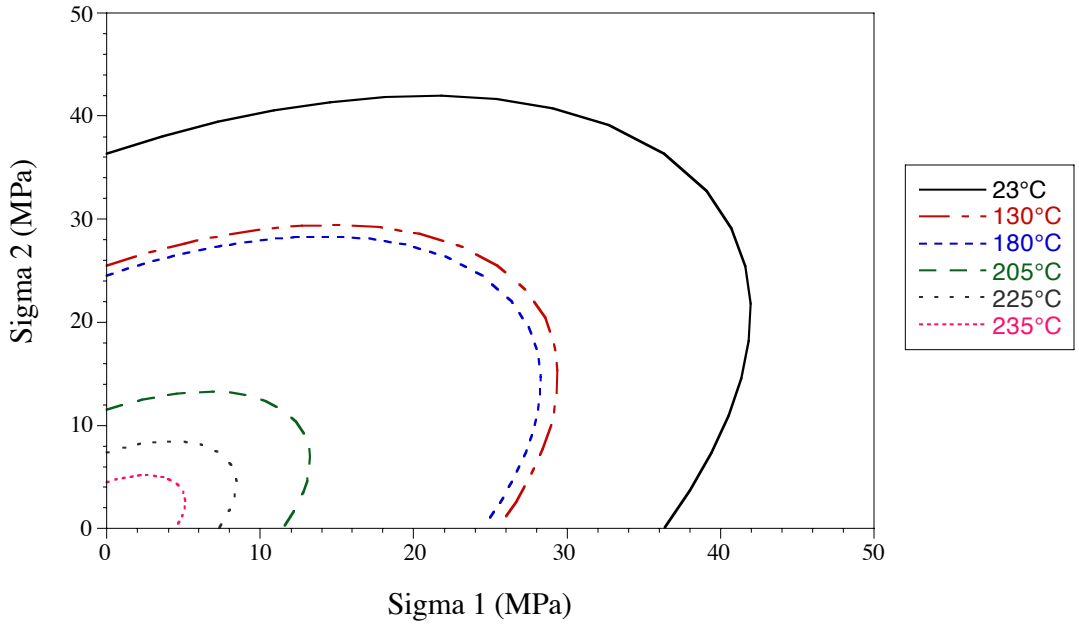

Figure 7: Yield surfaces for material with 1% molecular weight offset.

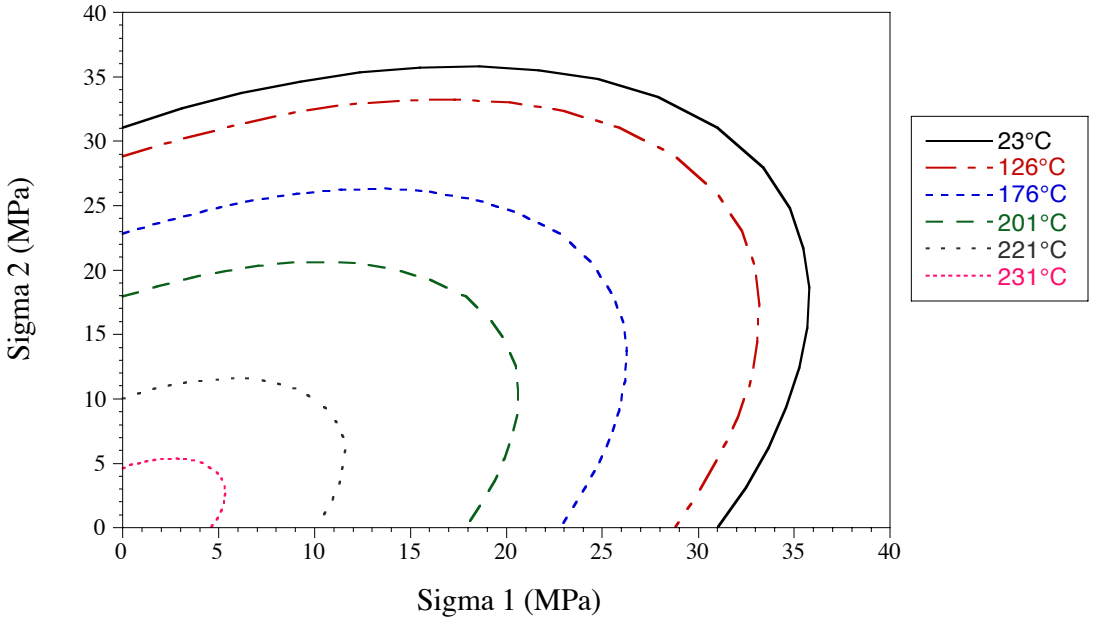

Figure 8: Yield surfaces for material with 2% molecular weight offset.

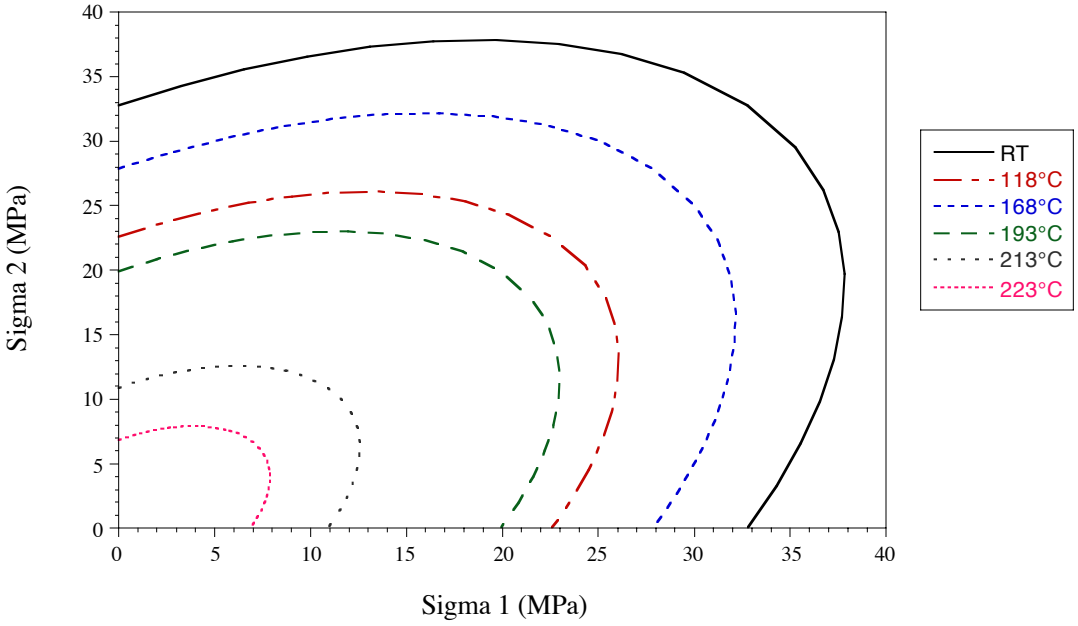

Figure 9: Yield surfaces for material with 3% molecular weight offset.

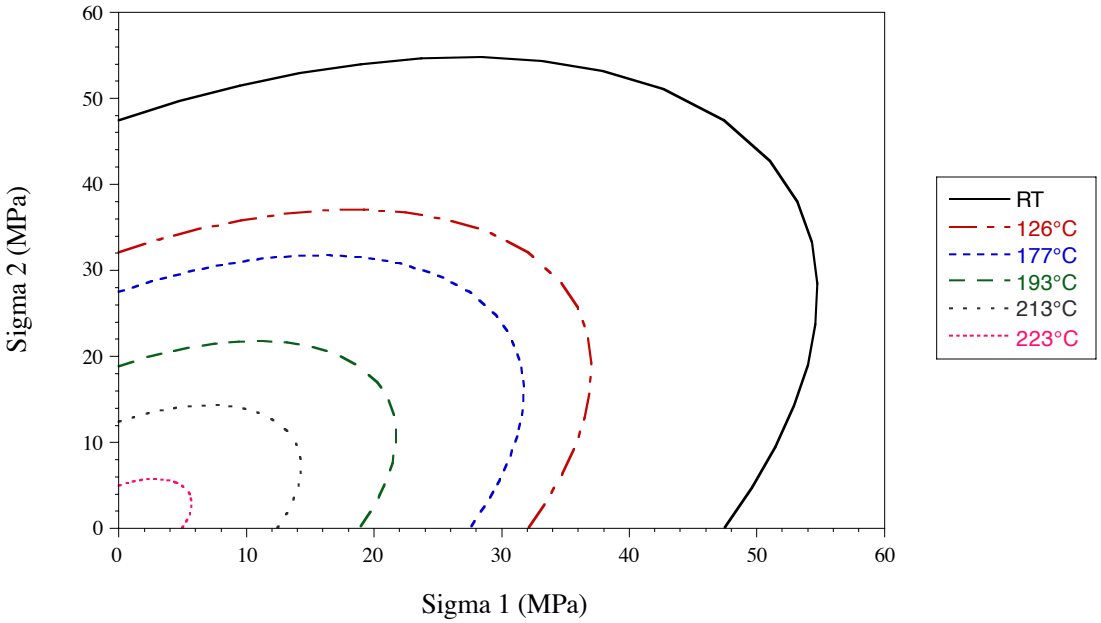

Figure 10: Yield surfaces for material with 4% molecular weight offset.

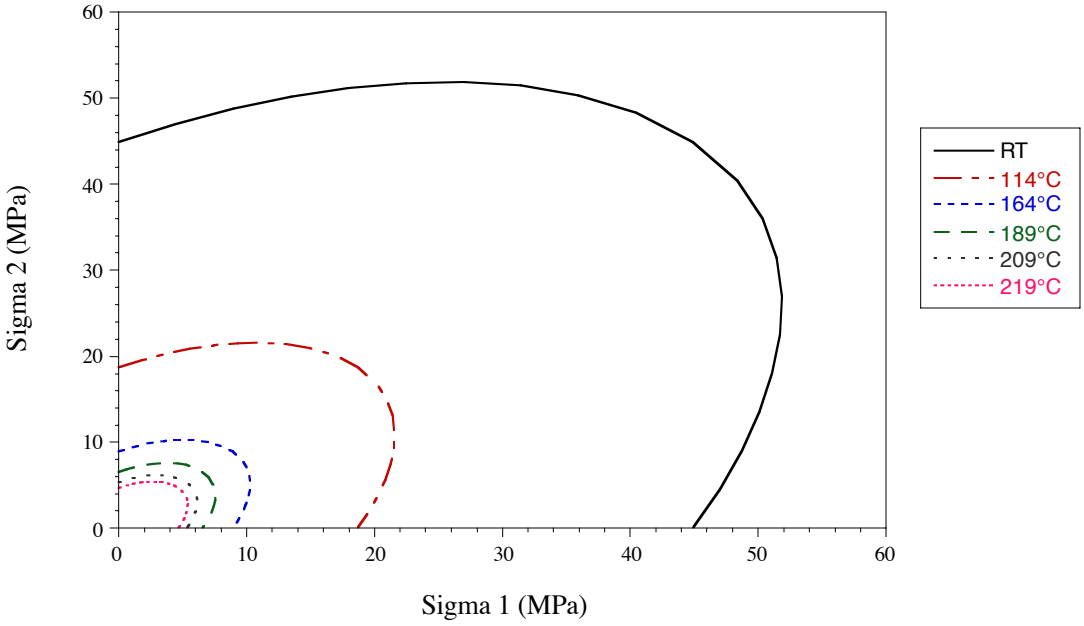

Figure 11: Yield surfaces for material with 5% molecular weight offset.

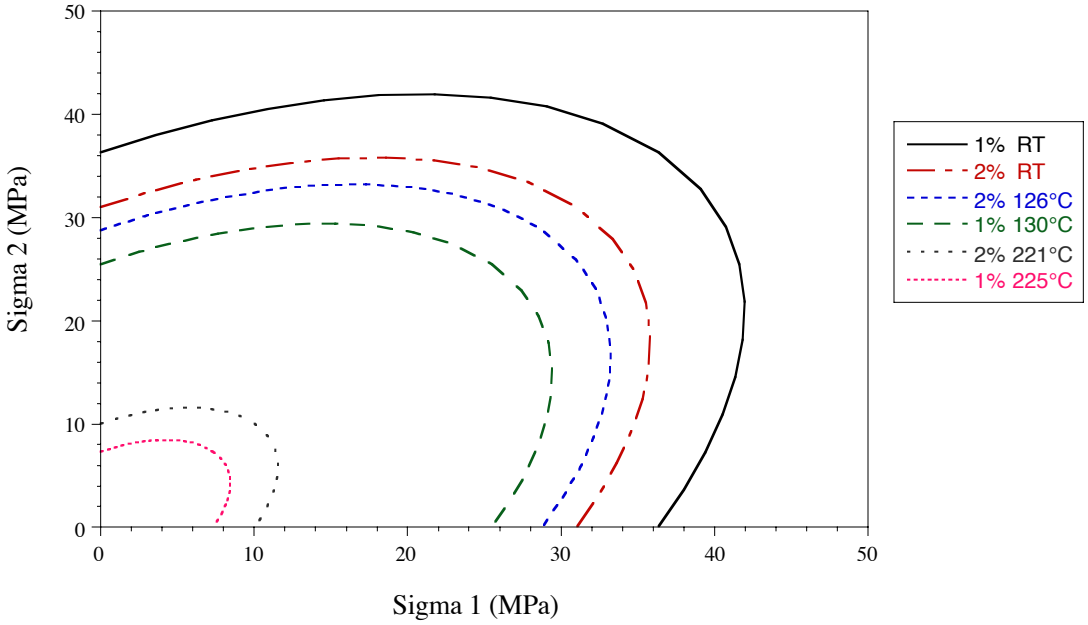

Figure 12: Yield surfaces for 1% molecular weight offset compared to 2% molecular weight offset at the same temperatures relative to their Tg's.

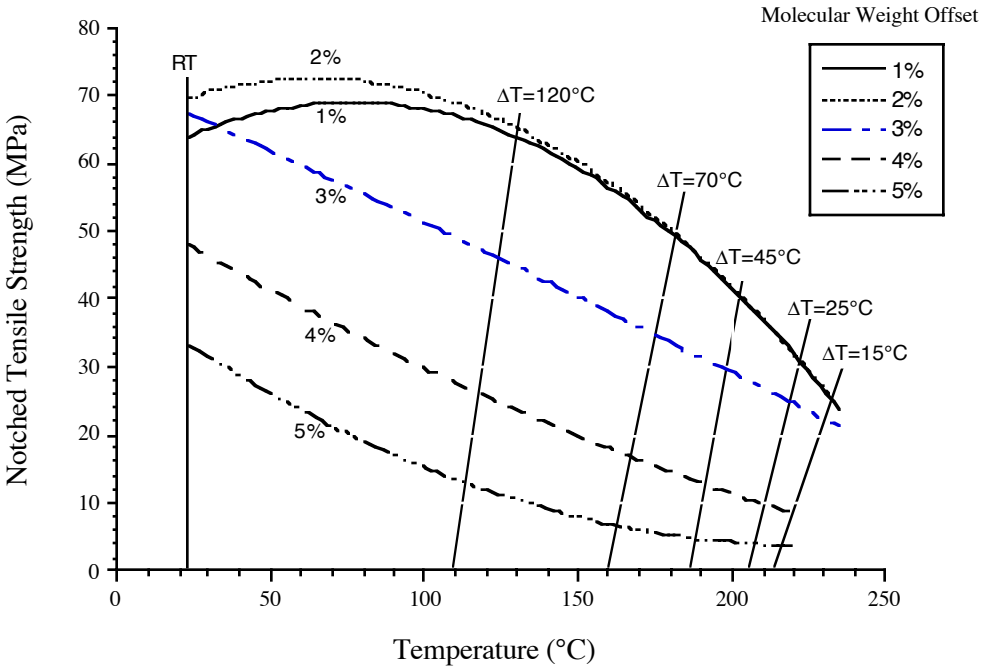

Figure 13: Notched Tensile Strength (MPa) as a function of test temperature.

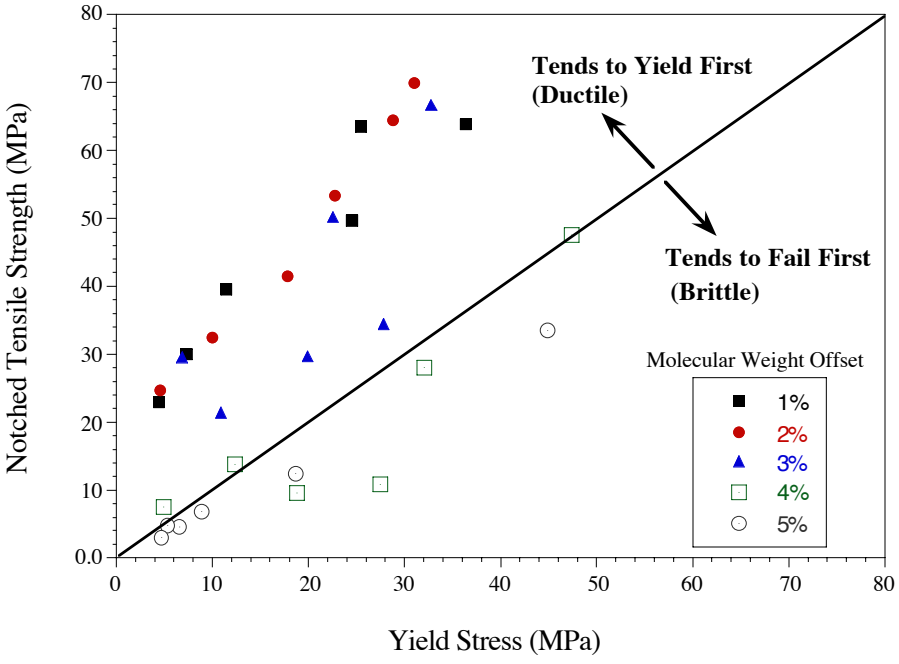

Figure 14: Notched Tensile Strength versus Yield Stress (MPa).

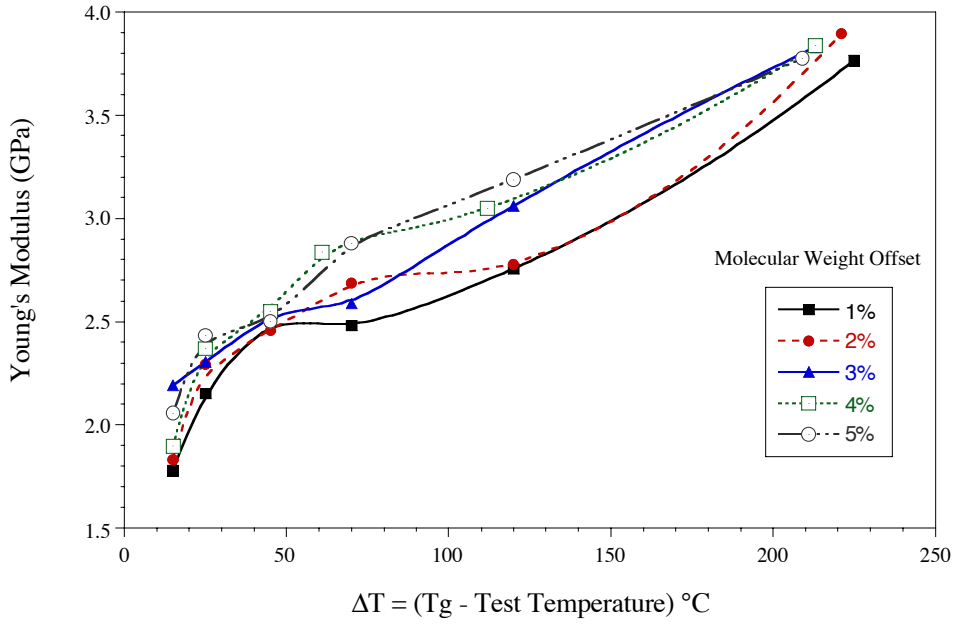

Figure 15: Dependence of Young's modulus on temperature.

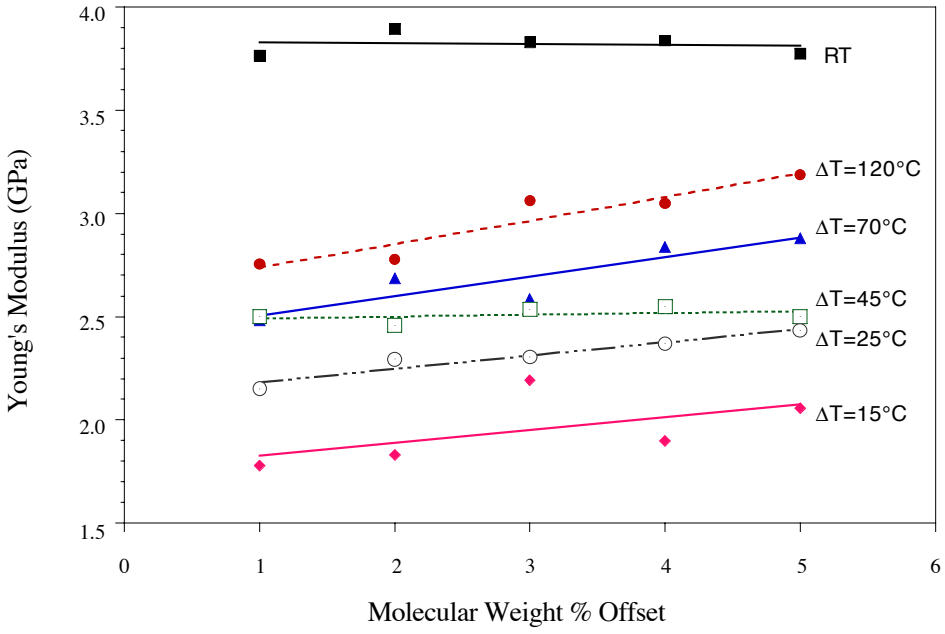

Figure 16: Dependence of Young's Modulus on molecular weight offset.

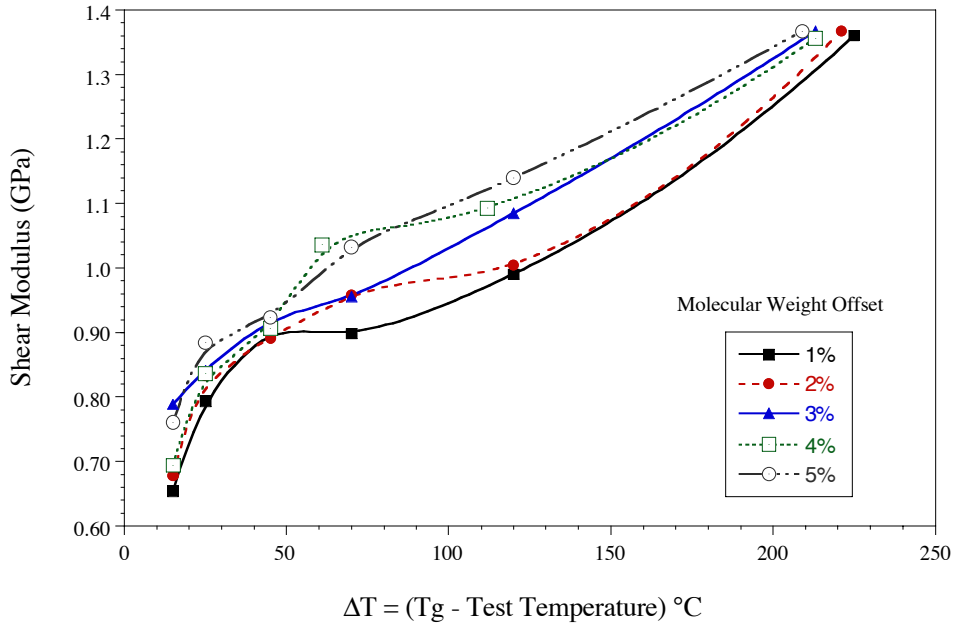

Figure 17: Dependence of shear modulus on temperature.

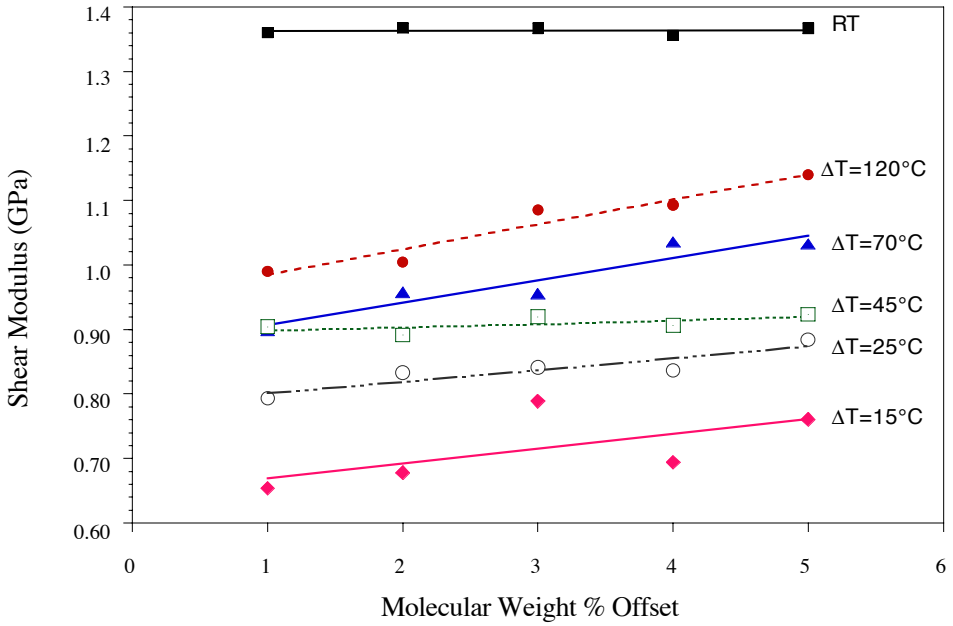

Figure 18: Dependence of shear modulus on molecular weight offset.

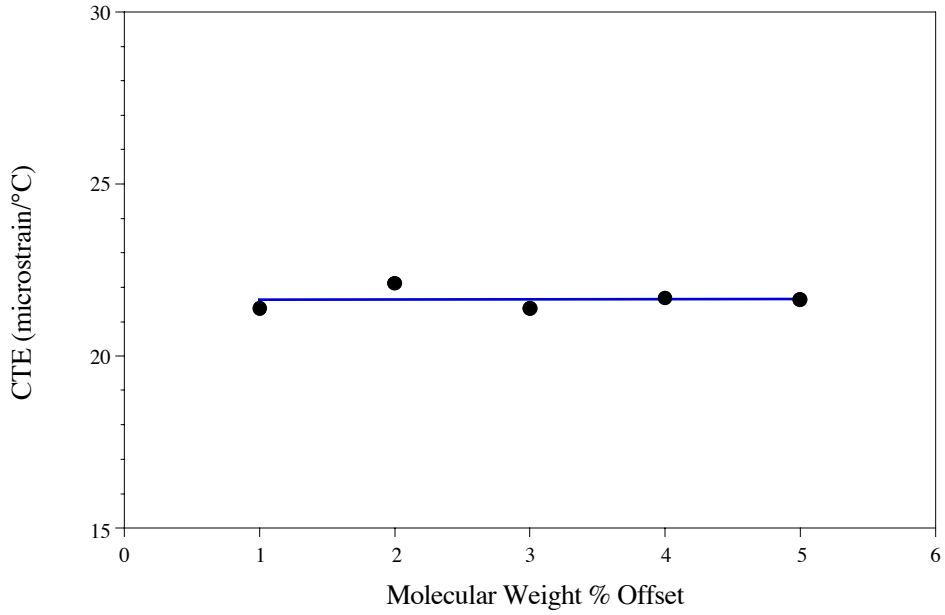

Figure 19: Variation of coefficient of thermal expansion with molecular weight percent offset.

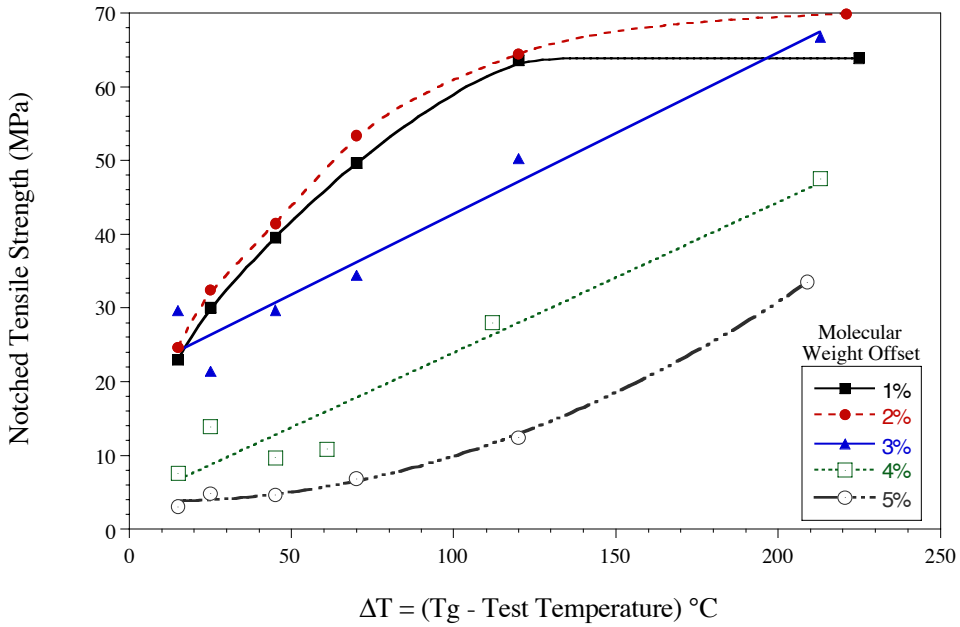

Figure 20: Notched tensile strength versus Δtemperature.

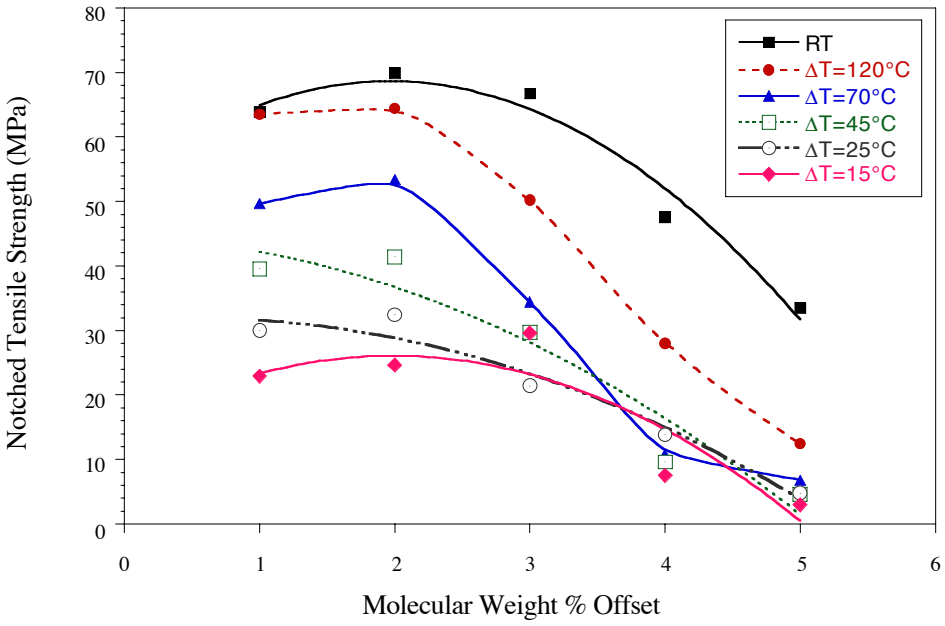

Figure 21: Dependence of notched tensile strength on molecular weight offset.

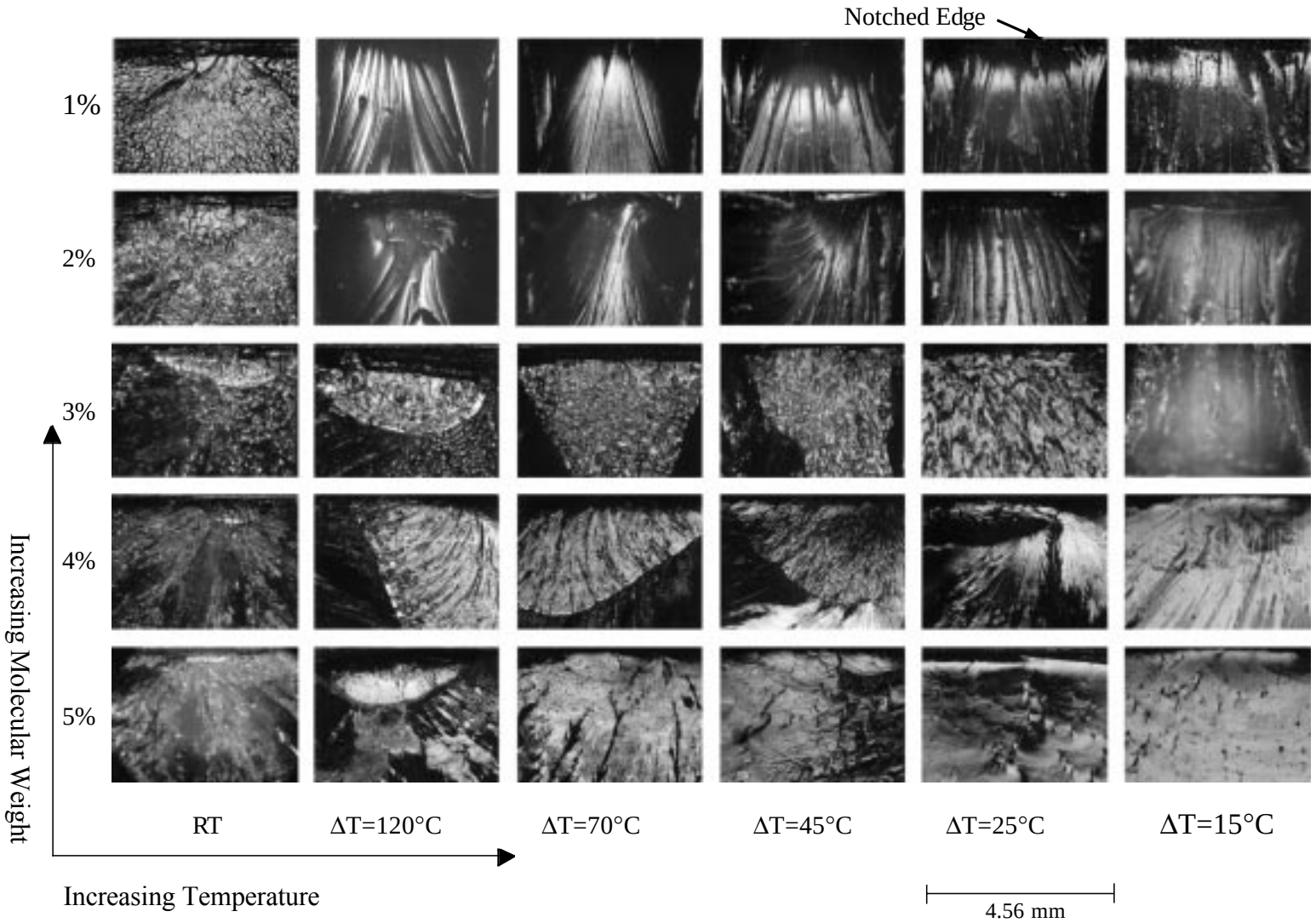

Figure 22: Photomicrographs of notched surface after failure.

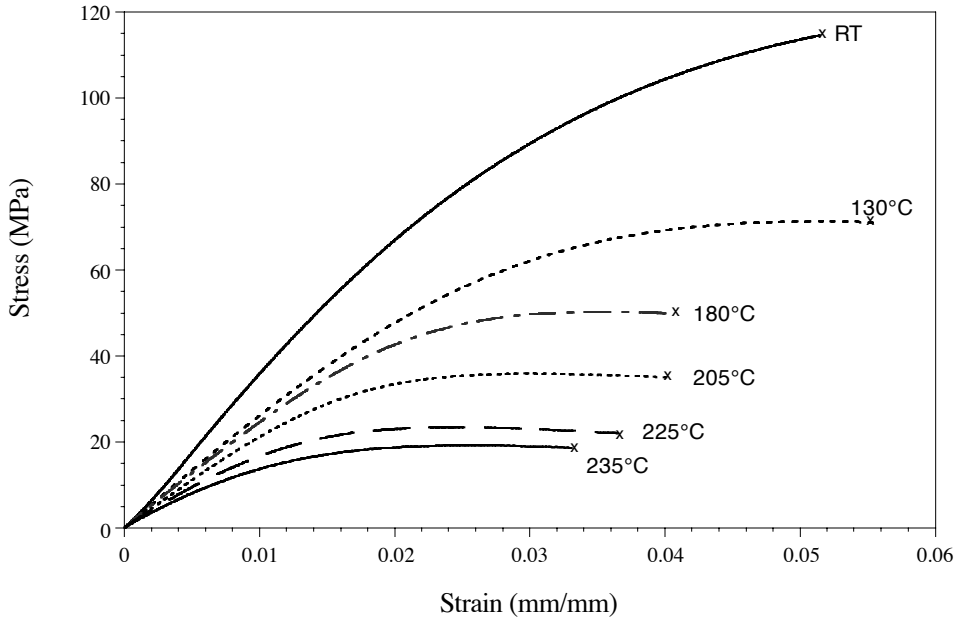

Figure 23: Stress versus strain of unnotched specimens with 1% molecular weight offset.

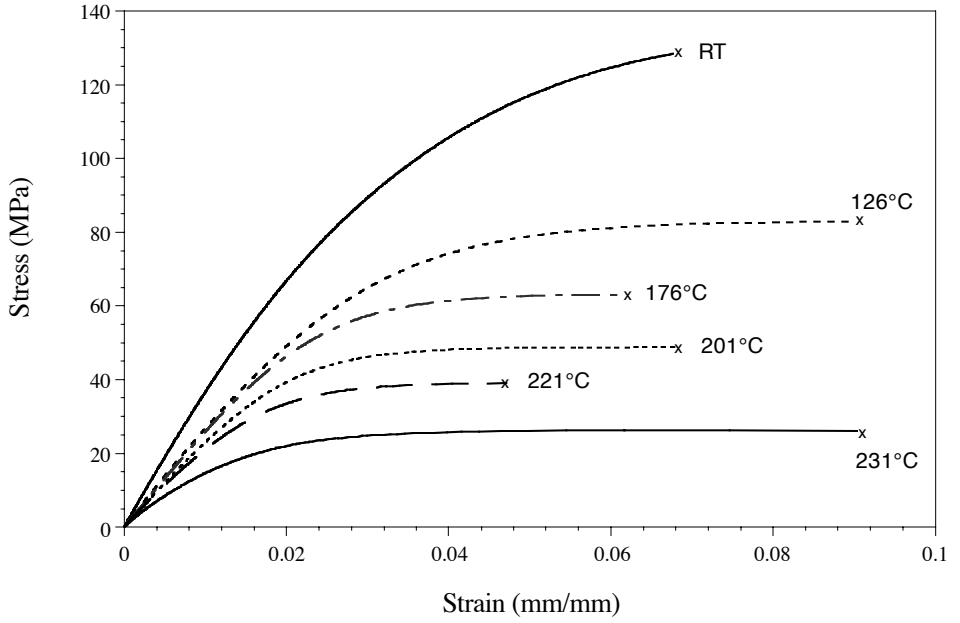

Figure 24: Stress versus strain of unnotched specimens with 2% molecular weight offset.

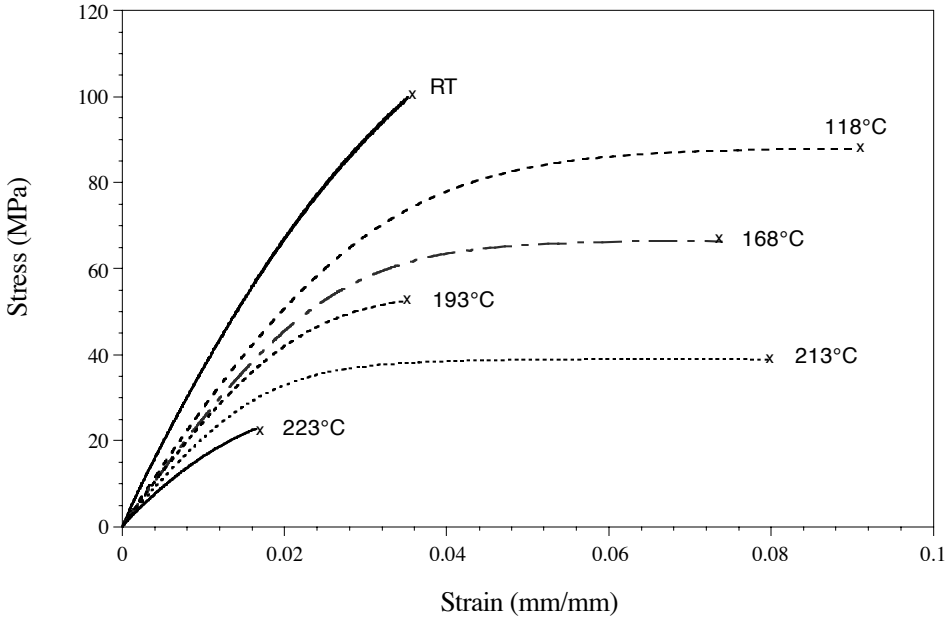

Figure 25: Stress versus strain of unnotched specimens with 3% molecular weight offset.

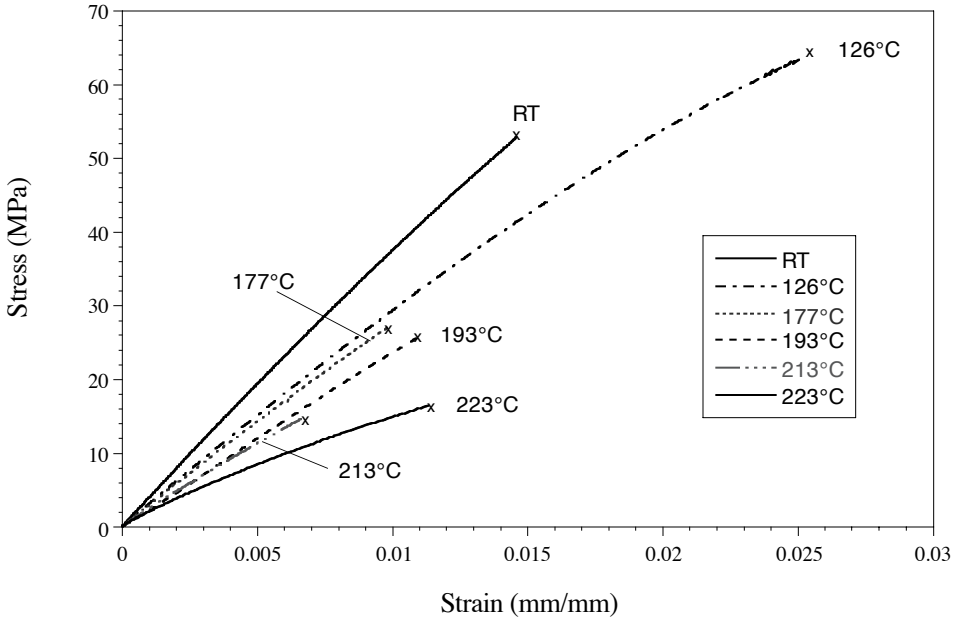

Figure 26: Stress versus strain of unnotched specimens with 4% molecular weight offset.

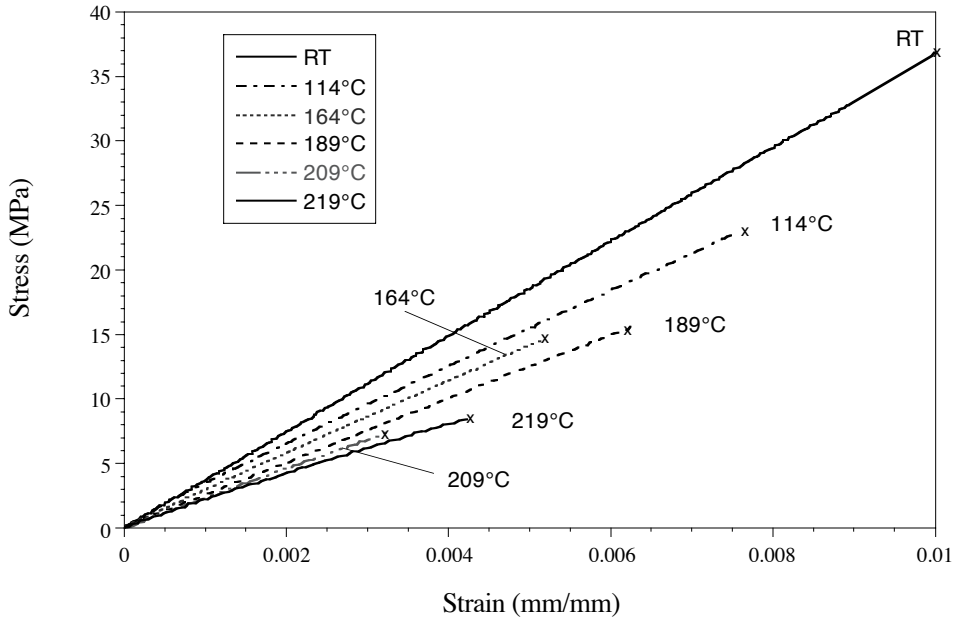

Figure 27: Stress versus strain of unnotched specimens with 5% molecular weight offset.

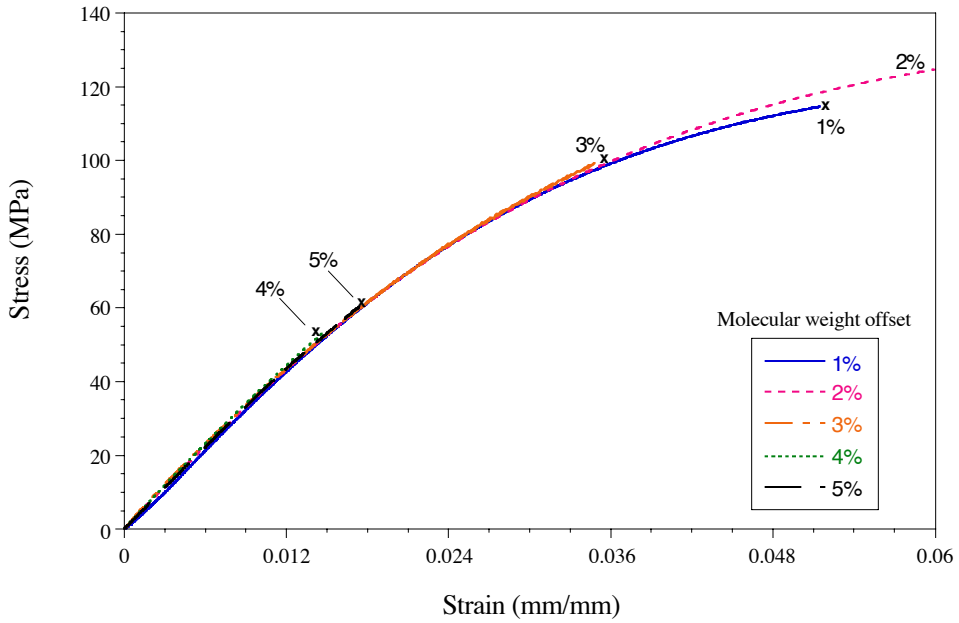

Figure 28: Stress versus strain of unnotched specimens tested at room temperature. Curves that terminate before 6% strain level indicate failure.

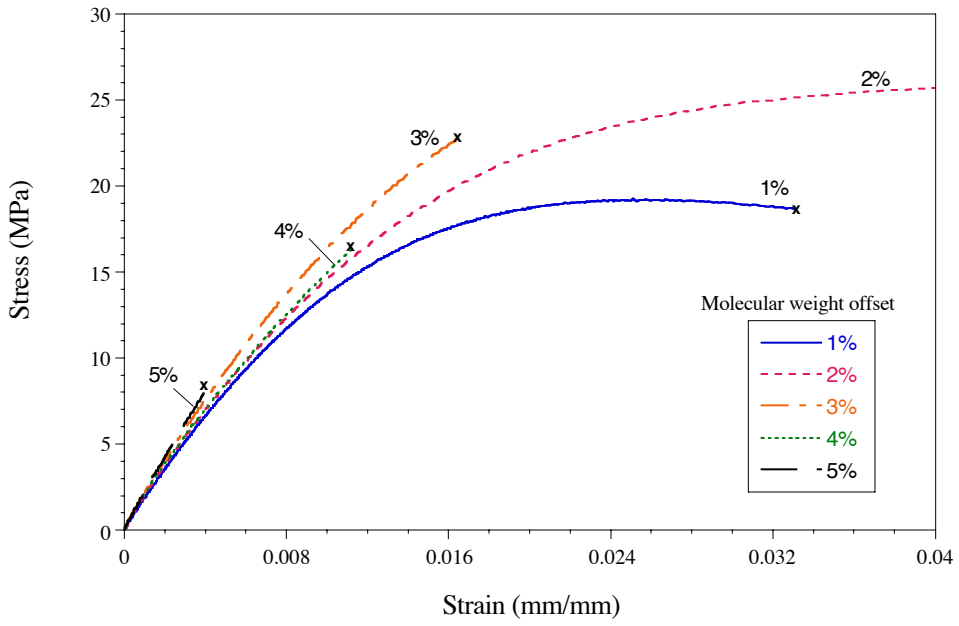

Figure 29: Stress versus strain of unnotched specimens tested at ΔT = 15°C (the highest test temperature). Curves that terminate before 4% strain level indicate failure.

REPORT DOCUMENTATION PAGE

Form Approved
OMB No. 0704-0188

1. AGENCY USE ONLY (Leave blank)	2. REPORT DATE	3. REPORT TYPE AND DATES COVERED
	August 2000	Technical Memorandum

4. TITLE AND SUBTITLE
Mechanical Properties of LaRC™ SI Polymer for a Range of Molecular Weights

5. FUNDING NUMBERS
WU 706-12-31-01

6. AUTHOR(S)
Karen S. Whitley, Thomas S. Gates, Jeffrey A. Hinkley, and Lee M. Nicholson

7. PERFORMING ORGANIZATION NAME(S) AND ADDRESS(ES)
NASA Langley Research Center
Hampton, VA 23681-2199

8. PERFORMING ORGANIZATION REPORT NUMBER
L-17993

9. SPONSORING/MONITORING AGENCY NAME(S) AND ADDRESS(ES)
National Aeronautics and Space Administration
Washington, DC 20546-0001

10. SPONSORING/MONITORING AGENCY REPORT NUMBER
NASA/TM-2000-210304

11. SUPPLEMENTARY NOTES
Whitley, Gates, and Hinkley: Langley Research Center, Hampton, VA
Nicholson: National Research Council Resident Research Associate, Langley Research Center, Hampton, VA

12a. DISTRIBUTION/AVAILABILITY STATEMENT
Unclassified-Unlimited
Subject Category 27 Distribution: Standard
Availability: NASA CASI (301) 621-0390

12b. DISTRIBUTION CODE

13. ABSTRACT (Maximum 200 words)
Mechanical testing of an advanced polyimide resin (LaRC™-SI) with known variations in molecular weight was performed over a range of temperatures below the glass transition temperature. Elastic and inelastic properties were characterized as a function of molecular weight and test temperature. It was shown that notched tensile strength is a strong function of both temperature and molecular weight, whereas stiffness is only a strong function of temperature. The combined analysis of calculated yield stress and notched tensile strength indicated that low molecular weight materials tended to fail in a brittle manner, whereas high molecular weight materials exhibited ductile failure. The microphotographs of the failure surfaces also supported these findings.

14. SUBJECT TERMS
polyimide; molecular weight; mechanical properties; notched tensile strength; yield stress; brittle-ductile transitions

15. NUMBER OF PAGES
35

16. PRICE CODE
A03

17. SECURITY CLASSIFICATION OF REPORT	18. SECURITY CLASSIFICATION OF THIS PAGE	19. SECURITY CLASSIFICATION OF ABSTRACT	20. LIMITATION OF ABSTRACT
Unclassified	Unclassified	Unclassified	UL